Simulations of Organic Aerosol Concentrations during Springtime in the Guanzhong Basin, China

Tian Feng[1,2,3], Guohui Li[2,3*], Junji Cao[2,3*], Naifang Bei[1,2], Zhenxing Shen[1], Weijian Zhou[3], Suixin Liu[2,3], Ting Zhang[2,3], Yichen Wang[2,3], Xuexi Tie[2,3], Luisa T. Molina[4]

[1]School of Human Settlements and Civil Engineering, Xi'an Jiaotong University, Xi'an, Shaanxi, China
[2]Key Lab of Aerosol Chemistry and Physics, Institute of Earth Environment, Chinese Academy of Sciences, Xi'an, Shaanxi, China
[3]State Key Laboratory of Loess and Quaternary Geology, Institute of Earth Environment, Chinese Academy of Sciences, Xi'an, China
[4]Molina Center for Energy and the Environment, La Jolla, CA, and Massachusetts Institute of Technology, Cambridge, MA, USA
[*]Correspondence to: Guohui Li (ligh@ieecas.cn) and Junji Cao (jjcao@ieecas.cn)

Abstract. The organic aerosol (OA) concentration is simulated in the Guanzhong basin, China from 23 to 25 April 2013 utilizing the WRF-CHEM model. Two approaches are used to predict OA concentrations: (1) a traditional secondary organic aerosol (SOA) module; (2) a non-traditional SOA module including the volatility basis-set modeling method in which primary organic aerosols (POA) are assumed to be semi-volatile and photochemically reactive. Generally, the spatial patterns and temporal variations of the calculated hourly near-surface ozone and fine particle matters agree well with the observations in Xi'an and surrounding areas. The model also yields reasonable distributions of daily $PM_{2.5}$ and elemental carbon (EC) compared to the filter measurements at 29 sites in the basin. Filter measured organic carbon (OC) and EC are used to evaluate OA, POA, and SOA using the OC/EC ratio approach. Compared with the traditional SOA module, the non-traditional module significantly improves SOA simulations and explains about 88% of the observed SOA concentration. Oxidation and partitioning of POA treated as semi-volatile constitute the most important pathway for the SOA formation, contributing more than 75% of the SOA concentrations in the basin. Residential emissions are the dominant anthropogenic OA source, constituting about 50% of OA concentrations in urban and rural areas and 30% in the background area. The OA contribution from transportation emissions decreases from 25% in urban areas to 20% in the background area, and the industry emission OA contribution is less than 6%.

Keywords: SOA, $PM_{2.5}$, WRF-CHEM Model

1 Introduction

Atmospheric aerosol or fine particulate matter ($PM_{2.5}$) influences regional and global climate directly by absorbing and scattering the solar radiation and indirectly by serving as cloud condensation nuclei (CCN) and ice nuclei (IN) to modify cloud properties (Seinfeld and Pandis, 2006). Elevated aerosol concentrations also exert adverse impacts on ecosystems and human health, and reduce the visibility of the atmosphere to cause the haze formation, impairing air quality (Cao et al., 2012a; 2012b; Greenwald et al., 2006; Seinfeld and Pandis, 2006).

OA constitutes one of the most important components of $PM_{2.5}$ in the atmosphere, with the mass contribution to $PM_{2.5}$ ranging from 20% to 90% (Kanakidou et al., 2005; Zhang et al., 2007). Traditionally, OA is categorized into primary and secondary OA on the basis of its source and/or formation, referred to as POA and SOA, respectively. POA is emitted into the atmosphere directly, while SOA forms through chemical reactions of precursors in the atmosphere. Volatile organic compounds (VOCs) emitted from anthropogenic or biogenic sources undergo a series of oxidation and gas-particle partitioning to yield SOA, which has been regarded as a traditional pathway of the SOA formation (Odum et al., 1996; Pankow, 1994). Recently, semi-volatile POA has been identified to be oxidized continuously to produce SOA in laboratory studies (Lipsky and Robinson, 2006; Shrivastava et al., 2006). The mechanism has been parameterized into chemical transport models (Dzepina et al., 2009; Lane et al., 2008; Li et al., 2011b; Murphy and Pandis, 2009; Robinson et al., 2007; Shrivastava et al., 2008; Tsimpidi et al., 2010), significantly improving SOA simulations and capable for closing the gap between the calculated and observed SOA concentrations.

China has been suffering severe air pollution caused by rapid industrialization and urbanization (Cao et al., 2007; 2005; 2012b; Guinot et al., 2007; He et al., 2015; 2001; Shen et al., 2009; Tie et al., 2015; Yang et al., 2011; Zhang et al., 2015; 2013). Numerous studies have shown that OA plays an important role in the haze formation in China. Huang et al. (2014) have reported that OA constitutes a major fraction (30~50%) of the total $PM_{2.5}$ in Beijing, Shanghai, Guangzhou, and Xi'an during severe haze pollution events (Table 1), and SOA contributed 44~71% of OA mass concentrations. Using the ACSM (Aerosol Chemical Speciation Monitor) measurements analyzed by PMF (positive matrix factorization), Sun et al. (2012) have showed that the oxygenated organic aerosols (OOA, a surrogate of SOA) dominate OA composition in Beijing, with a contribution of 64% on average from 26 June to 28 August 2011. Sun et al. (2013) have found that OA account for 52% of the total non-refractory submicron particulate matters mass loading measured by ACMS during 2012 wintertime in Beijing. Cao et al. (2013) have reported that secondary organic carbon constitutes 31% of the total carbon utilizing an EC tracer system and isotope mass balance calculations during the MIRAGE-Shanghai (Megacities Impact on Regional and Global Environment) campaign in 2009.

The Guanzhong basin (GZB) is located in northwestern China and nestled between the Qinling Mountains on the south and the Loess Plateau on the north (Figure 1), with a warm-humid climate. The rapid increasing industries and city expansions, as well as the unique topography, have caused frequent occurrence of haze events in GZB (Shen et al., 2009; 2008). Measurements have shown that carbonaceous aerosols (OA and EC) constitute 48.6% and 45.9% of $PM_{2.5}$ mass concentration in fall and winter, respectively in Xi'an, the largest city of GZB (Cao et al., 2005). Abundant OA has been reported to be directly emitted into the atmosphere from anthropogenic emissions, such as residential and transportation sources in GZB (Cao et al., 2005). High SOA levels have been observed in GZB during wintertime (Huang et al., 2014). However, the source and formation of OA and especially SOA in GZB still remain obscure.

During the period from 20 to 26 April 2013, a field campaign has been conducted to identify the OA distribution and sources in GZB and, due to occurrence of precipitation on the first three days, an episode during 23-25 April has been simulated to identify the OA sources in this study. Daily filter measurements at 29 sites in GZB have been collected, and EC and OC have been analyzed in $PM_{2.5}$. In general, the OC/EC ratio approach can be used to evaluate the OA, POA, and SOA concentrations using the filter measured OC and EC (Strader, 1999; Cao et al., 2003; 2004). Therefore, those measurements provide a good opportunity for better understanding OA sources and SOA formation in GZB.

The objective of the present study is to examine the formation and source apportionments of OA and SOA in GZB during three days in the spring of 2013 using the WRF-CHEM model. The WRF-CHEM model and its configuration are described in Section 2. The model results and discussions are presented in Section 3, and the conclusions are summarized in Section 4.

2 Model and Method

The WRF-Chem model and the SOA modules in the present study are nearly the same as those in Li et al. (2011b), which are briefly introduced in Sections 2.1 and 2.2 for convenience.

2.1 WRF-CHEM Model

A specific version of the WRF-CHEM model (Grell et al., 2005) developed by Li et al. (2010; 2011a; 2011b; 2012) at Molina Center for Energy and the Environment (MCE2) is utilized to investigate the OA formation in GZB. This version employs a flexible gas-phase chemical module and the CMAQ (version 4.6) aerosol module developed by US EPA (Binkowski and Roselle, 2003). The dry deposition of chemical species is parameterized according to Wesely (1989) and the wet deposition follows the method in CMAQ. The FTUV module (Li et al., 2005; Tie et al., 2003) considering the impacts of aerosols and clouds on photochemistry is used to calculate the photolysis rates. The ISORROPIA Version 1.7 (Nenes et al., 1998) is employed to the WRF-CHEM model to simulate the inorganic aerosols.

2.2 Secondary Organic Aerosol Modules

Two kinds of SOA modules are utilized in the WRF-CHEM model simulations: a traditional 2-product SOA module (T2-SOA module) and a non-traditional SOA module (NT-SOA module) (Li et al., 2011b).

In the T2-SOA module, SOA concentrations are predicted from the oxidation of six lumped organic species, including alkanes, alkenes, cresol, high-yield aromatics, low-yield aromatics, and monoterpenes, following the method developed by Schell et al. (2001).

The NT-SOA module simulates SOA formation based on the volatility basis-set (VBS) method (Donahue et al., 2006; Robinson et al., 2007). In the module, the POA is distributed in logarithmically spaced volatility bins and assumed to be semi-volatile and photochemically reactive (Li et al., 2011b). Nine surrogate species with saturation concentration ranging from 10^{-2} to 10^{6} μg m^{-3} at room temperature are selected to represent POA components following (Shrivastava et al., 2008). The SOA formation from glyoxal and methlyglyoxal is parameterized as a first-order irreversible uptake by aerosol particles with a reactive uptake coefficient of 3.7×10^{-3} (Volkamer et al., 2007; Zhao et al., 2006). Detailed information about T2-SOA and NT-SOA modules can be found in Li et al. (2011b).

2.3 Model Configuration

In this study, a three-day episode from 23 to 25 April 2013 is simulated in association with the filter measurements of $PM_{2.5}$, OC, and EC in GZB. The model is configured with a horizontal grid spacing of 3 km and 200 × 200 grid cells which is centered at 34.25°N and 109°E (Figure 1). In the vertical direction, we use thirty-five levels in a stretched vertical grid with spacing ranging from 50 m near the surface to 500 m at 2.5 km above ground level and

1 km above 14 km. The physics and dynamics of the configuration adopt the microphysics scheme of Hong and Lim (2006), the Yonsei University planetary boundary layer scheme (Hong et al., 2006), the land surface scheme of 5-layer thermal diffusion (Dudhia, 1996), the Dudhia shortwave scheme (Dudhia, 1989) and the rapid radiative transfer model (RRTM) longwave scheme (Mlawer et al., 1997). No cumulus parameterization is used due to the high horizontal resolution. The distance of GZB from the boundaries of the domain is about 150-200 km (50-70 grid cells). The NCEP 1°×1° reanalysis data are used for the meteorological initial and boundary conditions. In the present study, the NCEP ADP Global Surface Observational Weather Data (http://rda.ucar.edu/) in GZB are assimilated in the WRF-CHEM model simulations using the four-dimension data assimilation (FDDA) to improve the simulation of meteorological fields. The chemical initial and boundary conditions are interpolated from Model for OZone And Related chemical Tracers (MOZART) output with a 6-hour interval (Horowitz et al., 2003). The spin-up time for the simulation is one day.

The anthropogenic emission inventory (EI) including agriculture, industry, power plant, residential, and transportation sources is developed by Zhang et al. (2009). The temporal resolution of the emissions is one-hour, and a weekly and a diurnal cycle are included in the emissions. Figure 2 shows the monthly POA and VOCs emissions in GZB during April along with the Xi'an urban area. Large anthropogenic emissions are concentrated in Xi'an and surrounding areas. Table 2 presents the primary organic carbon and volatile organic compounds emissions from anthropogenic sources in Xi'an and surrounding areas in April. The POA from the transportation source and biomass burning are redistributed following Tsimpidi et al. (2010). The MEGAN model is used to on-line calculate the biogenic emissions in the model (Guenther et al., 2006).

2.4 Statistical Methods for Comparisons

The mean bias (*MB*), root mean square error (*RMSE*), and index of agreement (*IOA*) are used to evaluate the model performance in simulating gas-phase species and aerosols.

$$MB = \frac{1}{N}\sum_{i=1}^{N}(P_i - O_i) \tag{1}$$

$$RMSE = \left[\frac{1}{N}\sum_{i=1}^{N}(P_i - O_i)^2\right]^{\frac{1}{2}} \tag{2}$$

$$IOA = 1 - \frac{\sum_{i=1}^{N}(P_i - O_i)^2}{\sum_{i=1}^{N}\left(\left|P_i - \overline{O}\right| + \left|O_i - \overline{O}\right|\right)^2} \tag{3}$$

where P_i and O_i are the predicted and observed variables, respectively. N is the total number of the predictions for comparison and $\overline{O}$ donate the average of the observation. The *IOA* ranges from 0 to 1, with 1 showing a perfect agreement of the prediction with the observation.

2.5 Measurement Data

The measurement data include temperature, relative humidity, and wind observations at the Jinghe meteorological station, hourly near-surface O_3 and $PM_{2.5}$ concentrations at ambient monitoring stations in Xi'an and surrounding areas, and daily filter measurements of $PM_{2.5}$, OC, and EC at 29 sites in GZB during the field campaign and at Institute of Earth Environment, Chinese Academy of Sciences (IEECAS) in Xi'an during the springtime from 2009 to 2013. The observation sites are categorized into three types regarding their locations: 18 urban sites, 10 rural sites, and 1 background site as shown in Figure 1b. The background site is located in the Qinling Mountains, which is far away from the residential areas. The daily filter samples are obtained on prefired (900 °C, 3 h) 47-mm Whatman QM-A quartz-fiber filters by mini-volume air samplers (Airmetrics, Eugene, OR) at 5 L min^{-1} flow rates.

The measured $PM_{2.5}$ and OC concentrations averaged over the 29 sites in GZB during the study period are compared with the springtime $PM_{2.5}$ and OC observations at IEECAS site from 2009 to 2013 in Figure 3 along with the standard deviations. The springtime $PM_{2.5}$ concentrations at IEECAS site from 2009 to 2013 remain about 150 μg m^{-3} with small fluctuations, which is close to the $PM_{2.5}$ level during the study period. The springtime OC concentrations at IEECAS site from 2009 to 2013 vary from 14 μg m^{-3} to 22 μg m^{-3}. The mean OC concentration during the study period is about 19 μg m^{-3}, close to the medium level at IEECAS site from 2009 to 2013. Hence, the $PM_{2.5}$ and OC levels during the study period can well represent the springtime $PM_{2.5}$ and OC pollutions in GZB within recent years.

The OC/EC ratio approach has been widely employed to evaluate the OA concentration from the filter measured OC and EC concentrations (Strader, 1999; Cao et al., 2003; 2004). The following method is used to derive the "measured" POA, SOA, and OA mass concentrations from EC and OC filter measurements:

$$\mathrm{POC} = \mathrm{EC} \times (\mathrm{POC/EC\ ratio})$$

$$\mathrm{SOC} = \mathrm{OC} - \mathrm{POC}$$

$$\mathrm{POA} = \mathrm{POC} \times (\mathrm{POA/POC\ ratio})$$

$$\mathrm{SOA} = \mathrm{SOC} \times (\mathrm{SOA/SOC\ ratio})$$

$$\mathrm{OA} = \mathrm{POA} + \mathrm{SOA}$$

Cao et al. (2007) have analyzed the OC and EC concentrations in 14 cities over China in 2003 and proposed primary OC/EC ratios for different cities in China during winter and summer (Table 3). Numerous studies have been performed to investigate the POA/POC and SOA/SOC ratios (Aiken et al., 2008; Yu et al., 2009; Yu, 2011), which can be used to obtain OA concentrations from measured EC and OC concentrations. In this study, the POC/EC, POA/POC, SOA/SOC ratios are assumed to be 2.4, 1.2, and 1.6, respectively, based on the previous studies (Cao et al., 2007; Aiken et al., 2008; Yu et al., 2009; Yu, 2011). It is worth to note that, these assumed values might affect the model-measurement comparisons.

Using the measured EC and OC concentrations, the SOA/EC ratio is calculated:

(SOA/EC ratio) = (SOA/SOC ratio) × (SOC/EC ratio)

= (SOA/SOC ratio) × [(OC – POC) / EC]

= (SOA/SOC ratio) ×[(OC/EC ratio) – (POC/EC ratio)]

And the POA/EC ratio is derived as follows:

(POA/EC ratio) = (POA/POC ratio) × (POC/EC ratio)

3 Results and Discussions

3.1 Model Performance

The meteorological fields are of essential importance for the simulation of chemical species concentrations in time evolution and spatial distribution (Bei et al., 2008; 2010; 2012). Model performance is validated using the hourly ozone (O_3) and $PM_{2.5}$ observations at 13 monitoring sites in Xi'an and surrounding areas, released by the Ministry of Environmental Protection of China (China MEP), and daily filter measurement of $PM_{2.5}$, EC, and OC at 29 sites in GZB.

3.1.0 Meteorological Fields

Figure 4 shows comparisons of the simulated and observed near-surface temperature, relative humidity, wind speed and direction at the Jinghe meteorological station which is close to Xi'an (the yellow spot in Figure 1c) from 23 to 25 April 2013. The simulated diurnal variations of temperature and relative humidity are in good agreement with the observations. The model also generally well reproduces the wind field compared with observations, except overestimation of the wind speed during the daytime of April 23. No precipitation during the simulation period is observed or modeled.

3.1.1 Hourly O_3 and $PM_{2.5}$ Simulations in Xi'an and Surrounding Areas

Figures 5 and 6 provide the spatial patterns of observed and simulated near-surface O_3

and $PM_{2.5}$ mass concentrations at 08:00 and 15:00 Beijing Time (BJT) from April 23 to 25, 2013 in Xi'an and surrounding areas, along with simulated wind fields. The calculated O_3 and $PM_{2.5}$ spatial distributions are generally consistent with the observations at the monitoring sites. At 08:00 BJT, the weak near-surface winds and the low planetary boundary layer (PBL, not shown) facilitate the accumulation of pollutants, causing observed and simulated high near-surface $PM_{2.5}$ mass concentrations. The observed and calculated $PM_{2.5}$ mass concentration frequently exceeds 150 μg m^{-3}, causing heavy air pollution in Xi'an and surrounding areas. Weak solar insolation slows the photochemical activities and the low PBL is also favorable for buildup of emitted NO_x, significantly lowering the O_3 level at 08:00 BJT, and both the calculated and observed near-surface O_3 concentrations range from 20 to 30 μg m^{-3}. At 15:00 BJT, with the development of PBL and enhancement of horizontal winds, the $PM_{2.5}$ mass concentrations are decreased but still remain high level in Xi'an and surrounding areas on April 23 and 24. The simulated strong divergence at 15:00 BJT on April 25 efficiently disperses the $PM_{2.5}$ accumulated in the morning and remarkably improves the air quality in Xi'an and surrounding areas, which is also shown by the observed $PM_{2.5}$ concentrations. The observed and simulated O_3 mass concentrations substantially increase to more than 80 μg m^{-3} at 15:00 BJT with the enhancement of photochemical activities.

Figure 7 presents the temporal variations of calculated and measured O_3 and $PM_{2.5}$ concentrations averaged over 13 monitoring sites in Xi'an and surrounding areas from April 23 to 25, 2013. The WRF-CHEM model generally replicates the observed O_3 variations during the episode, i.e., the occurrence of peak O_3 concentrations in the afternoon due to active photochemical processes and rapid falloff during nighttime caused by the NO_x titration. The *MB* and *RMSE* are 7.1 μg m^{-3} and 21.3 μg m^{-3}, respectively, and the *IOA* is 0.89. The model considerably overestimates the observed O_3 concentration on April 23, perhaps due to the high O_3 background transport. However, on April 25, the model notably underestimates the peak O_3 concentration in the afternoon, which is caused by the simulated strong divergence in Xi'an and surrounding areas (Figure 5). Figure 7 shows that the variations of observed $PM_{2.5}$ are reasonably reproduced by the model, although overestimations and underestimations still exist. The *MB* and *RMSE* are 8.1 μg m^{-3} and 23.9 μg m^{-3}, respectively, and the *IOA* is 0.86. The observed and simulated $PM_{2.5}$ mass concentrations both show that during the three-day episode, the air quality with respect to $PM_{2.5}$ in Xi'an and surrounding areas gradually improves, with the $PM_{2.5}$ concentration decreased from about 160 μg m^{-3} in the morning on April 23 to about 50 μg m^{-3} in the afternoon on April 25. The $PM_{2.5}$ mass concentrations are generally elevated in the morning during the episode, probably contributed by the weak or calm horizontal winds, slow development of PBL, and the morning rush hour emissions. The $PM_{2.5}$ levels fall down in the afternoon, caused by the enhanced dispersion in the horizontal and vertical directions. The deviations between the model results and observations might be caused by the rapid changes in anthropogenic emissions that are not reflected in the current emission inventories, or the uncertainties in the meteorological filed simulations (Bei et al., 2008; 2010; 2012).

3.1.2 Daily $PM_{2.5}$ and EC Simulations in GZB

Daily filter measurements of $PM_{2.5}$ and EC mass concentrations at 29 sites in GZB (squares in Figure 1) are used to further verify the WRF-CHEM model simulations. Figure 8 shows the scatter plots of calculated and measured daily $PM_{2.5}$ and EC mass concentrations at 29 sites during the episode. The simulated daily $PM_{2.5}$ mass concentrations are generally in agreement with the filter measurement over 29 sites. The $PM_{2.5}$ concentration averaged over 29 sites during the episode is 79 μg m^{-3}, close to the observed 87 μg m^{-3}. The *MB* and *RMSE* of $PM_{2.5}$ mass concentrations are -7.4 μg m^{-3} and 10.3 μg m^{-3}, showing a reasonable $PM_{2.5}$ simulation in GZB. The WRF-CHEM model slightly overestimates the observed EC mass concentrations, with the *MB* of 0.2 μg m^{-3} and the *RMSE* of 0.6 μg m^{-3}.

The calculated daily spatial patterns of $PM_{2.5}$ and EC mass concentrations are displayed in Figure 9 along with the measurements at the 29 sites. The simulated distributions of $PM_{2.5}$ and EC mass concentrations are consistent with the filter measurements. On April 23, the eastern part of GZB is the most polluted area, with the daily $PM_{2.5}$ mass concentrations exceeding 115 μg m^{-3}. The daily $PM_{2.5}$ mass concentrations are still high on April 24, exceeding 75 μg m^{-3} over most of the area in GZB. The air quality in GZB is considerably improved on April 25, and the daily $PM_{2.5}$ mass concentrations are generally less than 75 μg m^{-3} in the north part of GZB. The EC distributions do not exhibit remarkable variations from April 23 to 25, indicating that the EC levels are primarily determined by direct emissions. In addition, although the daily $PM_{2.5}$ mass concentrations decrease substantially from April 23 to 25, the variations of EC mass concentrations are not so significant.

The WRF-CHEM model generally well reproduces O_3 and $PM_{2.5}$ concentrations in Xi'an and surrounding areas, and the daily EC and $PM_{2.5}$ mass concentrations in GZB, indicating that meteorological fields are well simulated and the emissions used are also reasonable in the study.

3.2 Organic Aerosols in GZB

3.2.1 OA Simulations from the T2-SOA and NT-SOA modules

Figure 10a shows that the scatterplot of the observed and simulated OA concentrations at 29 sites during the episode. The T2-SOA and NT-SOA modules exhibit differently in simulating OA in GZB, as shown in Figure 10a. The T2-SOA module overestimates the observed OA concentrations by about 33.6% averaged over the 29 sites, and the NT-SOA modules underestimates the observation by about 4.3%. Although the T2-SOA and NT-SOA modules both reproduce comparable OA levels against the measurements, the simulated OA components, i.e. POA and SOA, differ greatly between the two modules. Figures 10b and 10c provide comparisons of the simulated POA and SOA concentrations from the T2-SOA and NT-SOA modules with the measurements, respectively. The T2-SOA module overestimates the measured POA by around 132.0%, and only explains about 9.4% of the observed SOA concentration; the SOA underestimation of the T2-SOA module reaches a factor of 10. The SOA simulations are comparable to Li et al. (2011b), in which the T2-SOA module fails to yield sufficient SOA concentrations to match the observations by a factor of 7. As a comparison, the NT-SOA module overestimates the observed POA by 17.5% and explains around 87.7% of the observed SOA concentration, significantly improving the POA and SOA simulations. The NT-SOA module produces higher SOA than the T2-SOA module because the total amount of material (POA + Semivolatile-VOC + Intermediate-VOC) included in the NT-SOA module is 7.5 times the particle-phase POA emissions, which is consistent with the conclusion obtained by Li et al. (2011). Besides, many studies have already shown that the VBS approach produces higher SOA than the traditional 2-product SOA module (e.g., Hodzic et al., 2009; Tsimpidi et al., 2010).

The simulated POA/EC and SOA/EC ratios using NT-SOA module are 3.23 and 2.23, close to the “measured” 2.88 and 2.58, respectively. However, the simulations using T2-SOA module are 6.54 and 0.22, respectively, dramatically deviated from the “measurements”.

Figure 11 presents the temporal variations of simulated SOA mass concentrations in Xi’an and surrounding areas from the T2-SOA and NT-SOA modules, respectively. Both the two modules produce peak SOA concentrations around noontime, but, apparently, the NT-SOA module yields much more SOA than the T2-SOA module because the NT-SOA module contains more precursors and production processes. The NT-SOA module remarkably improves the SOA yields during the entire episode to around 7.2 μg m^{-3} compared with the observed SOA of 8.2 μg m^{-3} averaged over the 29 sites, about tenfold increase compared with the simulations from the T2-SOA module (0.77 μg m^{-3}).

3.2.2 Urban, Rural and Background POA and SOA

The NT-SOA module significantly improves POA and SOA simulations, so we use the NT-SOA OA simulations for further comparisons and OA source apportionment. Figure 12 displays the spatial distributions of OA, POA, and SOA simulated by the NT-SOA module against the measurement in GZB. The simulated OA, POA, and SOA patterns are generally in agreement with the observations, but the model frequently underestimates the observations in the north part of GZB (Figure 12). Both the simulation and the measurement show that the entire GZB is OA contaminated during the simulation episode (20 μg m^{-3} and above) (Figures 12a-c). POA is primarily concentrated in the central part of GZB, directly linked to the source region (Figures 12d-f). However, SOA is dispersed efficiently in the horizontal direction, showing the rapid aging process of OA. The simulations reveal a progressive increase of SOA concentrations in background areas, which is consistent with the measurements at the background site (red squares in Figures 12g-i).

The comparisons of the calculated and measured SOA mass fractions in OA at urban, rural and background sites using the NT-SOA module are displayed in Figure 13. The average mass fractions over each type of the sites are colored red. The mass fractions of SOA in OA at urban and rural sites are very close (around 44%~50% from the observations and around 40% from the simulation on average), suggesting a similar OA aging process in urban and rural areas of GZB. The SOA mass fraction at the background site is much higher, which well agrees with the observations (around 85% from the observations and around 70% from the simulation on average), indicating that the OA in background areas undergoes long-time aging processes.

The SOA formation pathways considered in the NT-SOA module include (1) oxidation of anthropogenic VOCs (ASOA), (2) oxidation of biogenic VOCs (BSOA), (3) oxidation and partitioning of POA treated as semi-volatile (PSOA), and (4) irreversible uptake of glyoxal and methylglyoxal on aerosol surfaces (GSOA). The SOA mass fractions in OA increase from 32.5%~37.3% at urban sites to 36.3%~44.1% at rural sites, and sharply to 58.6%~75.7% at the background site (Table 4). PSOA dominate SOA mass concentrations at all sites, and its contribution to SOA increases from 77.9%~79.5% at urban sites to 86.9%~89.4% at the background site, showing the continuous aging process of OA (Figure 14). The SOA contribution from ASOA and GSOA decreases from urban sites to the background site, showing the abatement of direct anthropogenic impacts. At urban sites, ASOA, BSOA, and GSOA contribute comparably to the SOA mass concentration. At the background site, the SOA contribution from ASOA and GSOA is very low, less than 4%. The GSOA constitutes about 5%~10% of SOA mass in the afternoon at urban sites, close to the 9.6% contribution of the observed SOA mass in urban area of Mexico City (Li et al., 2011b).

3.2.3 Contributions of Anthropogenic Emissions to OA

Sensitivity studies are conducted to estimate the contributions from anthropogenic emissions including industry, residential and transportation sources to the OA mass concentrations during the episode. The factor separation approach (FSA) proposed by Stein and Alpert (1993) is utilized to decompose the contribution from an individual source. The simulation with all anthropogenic emissions is taken as the base case (referred to as BAS case) to compare with the sensitivity studies. Four sensitivity studies are performed, including (1) ANT case without all anthropogenic emissions, (2) RES case without the residential emission, (3) IND case without the industry emission, and (4) TRA case without the transportation emission in simulations. According to the FSA approach, the OA contribution from an individual source, i.e., residential emissions, can be calculated as OA(BAS) – OA(RES).

Table 5 presents OA concentrations and contributions and OA contributions to $PM_{2.5}$ from anthropogenic emissions averaged over the simulation period at urban, rural, and background sites. During the simulation episode, anthropogenic emissions play a predominant role in the OA formation at the urban and rural sites, with the OA contribution of 82.4% (18.2 μg m^{-3}) and 77.3% (12.8 μg m^{-3}), respectively. At the background site, the OA contribution from anthropogenic emissions is close to 60% (4.7 μg m^{-3}), showing that the background area is still substantially influenced by human activities despite the far distance from the urban area. Residential emissions are the most important anthropogenic OA source at the urban and rural sites in the present study, with the OA contribution close to 50%, indicating that reducing residential emission is an efficient approach for OA mitigation in GZB. The OA contribution from the transportation source is 25.0% at the urban sites, exceeding 20.3% at the rural sites and 19.8% at the background sites. The industry emission is not an important OA source in GZB, with the contribution less than 6.1%. It is worth to note that, the OA contributions from residential, transportation, and industry emissions are comparable at the urban and rural sites, which probably is due to the rapid transport and transformation process between urban and rural areas. In addition, the urbanization and industrialization in GZB may also rapidly diminish the OA source difference between the rural and urban areas.

4 Summary and Conclusions

A 3-day episode from 23 to 25 April 2013 is simulated in the Guanzhong basin, China using the WRF-CHEM model to examine identify OA sources and SOA formation. We use two SOA approaches to simulate OA: a traditional 2-product SOA module and a non-traditional SOA module including VBS modeling method and the SOA contribution from dicarbonyl compounds. Meteorological observations during the simulation period are assimilated using the FDDA method in WRF-CHEM simulations. Model results are compared with the meteorological observations, hourly O_3 and $PM_{2.5}$ measurements in Xi'an and surrounding areas, and the $PM_{2.5}$ carbonaceous components from the OC and EC field filter measurements in GZB.

The WRF-CHEM model generally well simulates the spatial distributions and temporal variations of near-surface O_3 and $PM_{2.5}$, but biases still exist due to the uncertainties of meteorological fields and emission inventories. The model performs reasonably well in reproducing the distribution of the filter measured daily $PM_{2.5}$ and EC in GZB, but underestimates the observed $PM_{2.5}$ mass concentration by 7.4 μg m^{-3} on average.

The OC/EC ratio approach is used to evaluate OA, POA, and SOA concentrations from the filter measured OC and EC concentrations. The traditional and non-traditional SOA modules both yields reasonable OA simulations compared with measurements, but perform differently in simulating POA and SOA. The traditional module overestimates the measured POA concentration by around 132.0% but underestimates the observed SOA concentration by a factor of 10. The non-traditional module overestimates the observed POA concentration by 17.5% and explains around 87.7% of the observed SOA concentration, significantly improving the POA and SOA simulations. Although the model can produce similar $PM_{2.5}$ simulations when using the traditional and non-traditional SOA modules, the results might be misleading when the traditional SOA module is used to develop the $PM_{2.5}$ mitigation strategy.

Simulations from the non-traditional SOA module show that oxidation and partitioning of POA which is treated as semi-volatile in the model dominate the SOA concentration in GZB, with the SOA contribution exceeding 75% and also gradually increasing from urban sites to the background site. During the simulated period, the oxidation of anthropogenic and biogenic VOCs and the irreversible uptake of dicarbonyl compounds do not constitute an important SOA formation pathway in GZB, with the SOA contributions less than 10% generally. Anthropogenic emissions are the dominant OA source at urban and rural sites, contributing over 70% of OA concentrations. Residential emissions are the most important anthropogenic OA sources, constituting about 50% of OA concentrations at urban and rural sites and 30.2% at the background site. Transportation emissions make up 25.0% of the OA concentrations at urban sites and decreasing to 19.8% at the background site. The OA contribution from industry emissions is less than 6.1% in GZB.

Although the WRF-CHEM model reasonably well predicts the patterns and variations of observed O_3, $PM_{2.5}$, and aerosol components, biases still exist. It is worth to note that many factors contribute to the OA and SOA simulation uncertainties, such as measurements, meteorology, emissions, SOA formation mechanisms and treatments et al.; even right modeling results might be caused by wrong reasons (e.g., right concentrations but wrong O/C ratios). To better simulate the SOA formation, the SOA mechanisms and treatments need further revising and improving to reasonably represent OA formation and development in the atmosphere, such as including the oxidation degree, rather than only nine surrogates categorized by saturation concentrations. Additionally, reducing uncertainties from meteorological fields simulations and emissions are also imperative to improve the SOA simulation. In addition to OA, other aerosol species, such as sulfate, nitrate, ammonium, and mineral dust, also play important roles in the haze formation. Further source appointment of those aerosol species is needed to support the design of mitigation strategies. It should be noted that, this simulation is conducted during 3 days in spring 2013, so it might be only partially representative of the springtime $PM_{2.5}$ and OC pollutions. Nevertheless, considering that the $PM_{2.5}$ and OC concentrations during the study period are similar to those in the past five years, the model result is still important and provides a reference for springtime OA formation.

Data availability: The real-time O_3 and $PM_{2.5}$ are accessible for the public on the website http://106.37.208.233:20035/. One can also access the historic profile of observed ambient pollutants through visiting http://www.aqistudy.cn/.

Acknowledgements. This work was supported by the National Natural Science Foundation of China (No. 41275153) and supported by the "Strategic Priority Research Program" of the Chinese Academy of Sciences，Grant No. XDB05060500. Guohui Li is also supported by the “Hundred Talents Program” of the Chinese Academy of Sciences. Naifang Bei is supported by the National Natural Science Foundation of China (No. 41275101).

References

Aiken, A. C., DeCarlo, P. F., Kroll, J. H., Worsnop, D. R., Huffman, J. A., Docherty, K. S., Ulbrich, I. M., Mohr, C., Kimmel, J. R., Sueper, D., Sun, Y., Zhang, Q., Trimborn, A., Northway, M., Ziemann, P. J., Canagaratna, M. R., Onasch, T. B., Alfarra, M. R., Prévôt, A. S. H., Dommen, J., Duplissy, J., Metzger, A., Baltensperger, U. and Jimenez, J. L.: O/C and OM/OC Ratios of Primary, Secondary, and Ambient Organic Aerosols with High-Resolution Time-of-Flight Aerosol Mass Spectrometry, Environ. Sci. Technol., 42(12), 4478–4485, doi:10.1021/es703009q, 2008.

Bei, N., de Foy, B., Lei, W., Zavala, M. and Molina, L. T.: Using 3DVAR data assimilation system to improve ozone simulations in the Mexico City basin, Atmos. Chem. Phys., 8(24), 7353–7366, doi:10.5194/acp-8-7353-2008, 2008.

Bei, N., Lei, W., Zavala, M. and Molina, L. T.: Ozone predictabilities due to meteorological uncertainties in the Mexico City basin using ensemble forecasts, Atmos. Chem. Phys., 10(13), 6295–6309, doi:10.5194/acp-10-6295-2010, 2010.

Bei, N., Li, G. and Molina, L. T.: Uncertainties in SOA simulations due to meteorological uncertainties in Mexico City during MILAGRO-2006 field campaign, Atmos. Chem. Phys., 12(23), 11295–11308, doi:10.5194/acp-12-11295-2012, 2012.

Binkowski, F. S. and Roselle, S. J.: Models-3 Community Multiscale Air Quality (CMAQ) model aerosol component 1. Model description, J. Geophys. Res., 108(D6), 4183–18, doi:10.1029/2001JD001409, 2003.

Cao, J. J., Lee, S. C., Chow, J. C., Watson, J. G., Ho, K. F., Zhang, R. J., Jin, Z. D., Shen, Z. X., Chen, G. C., Kang, Y. M., Zou, S. C., Zhang, L. Z., Qi, S. H., Dai, M. H., Cheng, Y. and Hu, K.: Spatial and seasonal distributions of carbonaceous aerosols over China, J. Geophys. Res., 112(D22), D22S11–9, doi:10.1029/2006JD008205, 2007.

Cao, J. J., Lee, S. C., Ho, K. F., Zhang, X. Y. and Zou, S. C.: Characteristics of carbonaceous aerosol in Pearl River Delta Region, China during 2001 winter period, Atmos. Environ., 37(11), 1451–1460, doi:10.1016/s1352-2310(02)01002-6, 2003.

Cao, J. J., Lee, S. C., Ho, K. F., Zou, S. C., Fung, K., Li, Y., Watson, J. G. and Chow, J. C.: Spatial and seasonal variations of atmospheric organic carbon and elemental carbon in Pearl River Delta Region, China, Atmos. Environ., 38(27), 4447–4456, doi:10.1016/j.atmosenv.2004.05.016, 2004.

Cao, J. J., Wu, F., Chow, J. C., Lee, S. C. and Li, Y.: Characterization and source apportionment of atmospheric organic and elemental carbon during fall and winter of 2003 in Xi'an, China, Atmos. Chem. Phys., 5(11), 3127–3137, doi:10.5194/acp-5-3127-2005, 2005.

Cao, J. J., Zhu, C. S., Tie, X. X., Geng, F. H., Xu, H. M., Ho, S. S. H., Wang, G. H., Han, Y. M. and Ho, K. F.: Characteristics and sources of carbonaceous aerosols from Shanghai, China, Atmos. Chem. Phys., 13(2), 803–817, doi:10.5194/acp-13-803-2013, 2013.

Cao, J., Xu, H., Xu, Q., Chen, B. and Kan, H.: Fine particulate matter constituents and cardiopulmonary mortality in a heavily polluted Chinese city, Environ. Health Perspect., 120(3), 373–378, doi:10.1289/ehp.1103671, 2012a.

Cao, J.-J., Wang, Q.-Y., Chow, J. C., Watson, J. G., Tie, X.-X., Shen, Z.-X., Wang, P. and An, Z.-S.: Impacts of aerosol compositions on visibility impairment in Xi'an, China, Atmos. Environ., 59, 559–566, doi:10.1016/j.atmosenv.2012.05.036, 2012b.

Donahue, N. M., Robinson, A. L., Stanier, C. O. and Pandis, S. N.: Coupled Partitioning, Dilution, and Chemical Aging of Semivolatile Organics, Environ. Sci. Technol., 40(8), 2635–2643, doi:10.1021/es052297c, 2006.

Dudhia, J.: Numerical study of convection observed during the winter monsoon experiment using a mesoscale two-dimensional model, J. Atmos. Sci., 46(20), 3077–3107, doi:10.1175/1520-0469(1989)046<3077:NSOCOD>2.0.CO;2, 1989.

Dudhia, J.: A multi-layer soil temperature model for MM5, Preprints, 49–50, 1996.

Dzepina, K., Volkamer, R. M., Madronich, S., Tulet, P., Ulbrich, I. M., Zhang, Q., Cappa, C. D., Ziemann, P. J. and Jimenez, J. L.: Evaluation of recently-proposed secondary organic aerosol models for a case study in Mexico City, Atmos. Chem. Phys., 9(15), 5681–5709, doi:10.5194/acp-9-5681-2009, 2009.

Greenwald, R., Bergin, M. H., Xu, J. and Cohan, D.: The influence of aerosols on crop production: A study using the CERES crop model, Agr. Syst., 89(2-3), 390–413, doi:10.1016/j.agsy.2005.10.004, 2006.

Grell, G. A., Peckham, S. E., Schmitz, R., McKeen, S. A., Frost, G., Skamarock, W. C. and Eder, B.: Fully coupled “online” chemistry within the WRF model, Atmos. Environ., 39(37), 6957–6975, doi:10.1016/j.atmosenv.2005.04.027, 2005.

Guenther, A., Karl, T., Harley, P., Wiedinmyer, C., Palmer, P. I. and Geron, C.: Estimates of global terrestrial isoprene emissions using MEGAN (Model of Emissions of Gases and Aerosols from Nature), Atmos. Chem. Phys., 6(11), 3181–3210, doi:10.5194/acp-6-3181-2006, 2006.

Guinot, B., Cachier, H., Sciare, J., Tong, Y., Xin, W. and Jianhua, Y.: Beijing aerosol: Atmospheric interactions and new trends, J. Geophys. Res., 112(D14), D14314–16, doi:10.1029/2006JD008195, 2007.

He, H., Tie, X., Zhang, Q., Liu, X., Gao, Q., Li, X. and Gao, Y.: Analysis of the causes of heavy aerosol pollution in Beijing, China: A case study with the WRF-Chem model, Particuology, 20, 32–40, doi:10.1016/j.partic.2014.06.004, 2015.

He, K., Yang, F., Ma, Y., Zhang, Q., Yao, X., Chan, C. K., Cadle, S., Chan, T. and Mulawa, P.: The characteristics of PM2.5 in Beijing, China, Atmos. Environ., 35(29), 4959–4970, doi:10.1016/S1352-2310(01)00301-6, 2001.

Hodzic, A., Jimenez, J. L., Madronich, S., Aiken, A. C., Bessag- net, B., Curci, G., Fast, J., Lamarque, J.-F., Onasch, T. B., Roux, G., Schauer, J. J., Stone, E. A., and Ulbrich, I. M.: Modeling organic aerosols during MILAGRO: importance of biogenic secondary organic aerosols, Atmos. Chem. Phys., 9, 6949–6981, doi:10.5194/acp-9-6949-2009, 2009.

Hong, S. Y. and Lim, J.: The WRF single-moment 6-class microphysics scheme (WSM6), Asia-Pac J. Atmos. Sci., 2006.

Hong, S. Y., Noh, Y. and Dudhia, J.: A new vertical diffusion package with an explicit treatment of entrainment processes, Mon. Weather Rev., 134(9), 2318–2341, doi:10.1175/mwr3199.1, 2006.

Horowitz, L. W., Walters, S. and Mauzerall, D. L.: A global simulation of tropospheric ozone and related tracers: Description and evaluation of MOZART, version 2, J. Geophys. Res., 108(D24), 4784, doi:10.1029/2002jd002853, 2003.

Huang, R.-J., Zhang, Y., Bozzetti, C., Ho, K.-F., Cao, J.-J., Han, Y., Daellenbach, K. R., Slowik, J. G., Platt, S. M., Canonaco, F., Zotter, P., Wolf, R., Pieber, S. M., Bruns, E. A., Crippa, M., Ciarelli, G., Piazzalunga, A., Schwikowski, M., Abbaszade, G., Schnelle-Kreis, J., Zimmermann, R., An, Z., Szidat, S., Baltensperger, U., Haddad, El, I. and Prévôt, A. S. H.: High secondary aerosol contribution to particulate pollution during haze events in China, Nature, 514(7521), 218–222, doi:10.1038/nature13774, 2014.

Kanakidou, M., Seinfeld, J. H. and Pandis, S. N.: Organic aerosol and global climate modelling: a review, Atmos. Chem. Phys., 5(4), 1053–1123, doi:10.5194/acp-5-1053-2005, 2005.

Lane, T. E., Donahue, N. M. and Pandis, S. N.: Simulating secondary organic aerosol formation using the volatility basis-set approach in a chemical transport model, Atmos. Environ., 42(32), 7439–7451, doi:10.1016/j.atmosenv.2008.06.026, 2008.

Li, G., Bei, N., Tie, X. and Molina, L. T.: Aerosol effects on the photochemistry in Mexico City during MCMA-2006/MILAGRO campaign, Atmos. Chem. Phys., 11(11), 5169–5182, doi:10.5194/acp-11-5169-2011, 2011a.

Li, G., Lei, W., Bei, N. and Molina, L. T.: Contribution of garbage burning to chloride and $PM_{2.5}$ in Mexico City, Atmos. Chem. Phys., 12(18), 8751–8761, doi:10.5194/acp-12-8751-2012, 2012.

Li, G., Lei, W., Zavala, M., Volkamer, R., Dusanter, S., Stevens, P. and Molina, L. T.: Impacts of HONO sources on the photochemistry in Mexico City during the MCMA-2006/MILAGO Campaign, Atmos. Chem. Phys., 10(14), 6551–6567, doi:10.5194/acp-10-6551-2010, 2010.

Li, G., Zavala, M., Lei, W., Tsimpidi, A. P., Karydis, V. A., Pandis, S. N., Canagaratna, M. R. and Molina, L. T.: Simulations of organic aerosol concentrations in Mexico City using the WRF-CHEM model during the MCMA-2006/MILAGRO campaign, Atmos. Chem. Phys., 11(8), 3789–3809, doi:10.5194/acp-11-3789-2011, 2011b.

Li, G., Zhang, R., Fan, J. and Tie, X.: Impacts of black carbon aerosol on photolysis and ozone, J. Geophys. Res., 110(D23), D23206–10, doi:10.1029/2005JD005898, 2005.

Lipsky, E. M. and Robinson, A. L.: Effects of Dilution on Fine Particle Mass and Partitioning of Semivolatile Organics in Diesel Exhaust and Wood Smoke, Environ. Sci. Technol., 40(1), 155–162, doi:10.1021/es050319p, 2006.

Mlawer, E. J., Taubman, S. J., Brown, P. D., Iacono, M. J. and Clough, S. A.: Radiative transfer for inhomogeneous atmospheres: RRTM, a validated correlated‐k model for the longwave, J. Geophys. Res., 102(D14), 16663–16682, doi:10.1029/97JD00237, 1997.

Murphy, B. N. and Pandis, S. N.: Simulating the Formation of Semivolatile Primary and Secondary Organic Aerosol in a Regional Chemical Transport Model, Environ. Sci. Technol., 43(13), 4722–4728, doi:10.1021/es803168a, 2009.

Nenes, A., Pilinis, C., Pandis, S. N.: ISORROPIA: A New Thermodynamic Equilibrium Model for Multiphase Multicomponent Inorganic Aerosols, Aquat. Geochem., 4(1), 123-152, http://nenes.eas.gatech.edu/ISORROPIA/, 1998.

Odum, J. R., Hoffmann, T. and Bowman, F.: Gas/particle partitioning and secondary organic aerosol yields, Environ. Sci. Technol., 30(8), 2580–2585, doi:10.1021/es950943, 1996.

Pankow, J. F.: An absorption model of gas/particle partitioning of organic compounds in the atmosphere, Atmos. Environ., 28(2), 185–188, doi:10.1016/1352-2310(94)90093-0, 1994.

Robinson, A. L., Donahue, N. M., Shrivastava, M. K., Weitkamp, E. A., Sage, A. M., Grieshop, A. P., Lane, T. E., Pierce, J. R. and Pandis, S. N.: Rethinking organic aerosols:

semivolatile emissions and photochemical aging, Science, 315(5816), 1259–1262, doi:10.1126/science.1133061, 2007.

Schell, B., Ackermann, I. J., Hass, H., Binkowski, F. S. and Ebel, A.: Modeling the formation of secondary organic aerosol within a comprehensive air quality model system, J. Geophys. Res., 106(D22), 28275–28293, doi:10.1029/2001jd000384, 2001.

Seinfeld, J. H. and Pandis, S. N.: Atmospheric Chemistry and Physics - From Air Pollution to Climate Change, 2nd ed., John Wiley & Sons, New Jersey. 2006.

Shen, Z., Arimoto, R., Cao, J., Zhang, R. and Li, X.: Seasonal Variations and Evidence for the Effectiveness of Pollution Controls on Water-Soluble Inorganic Species in Total Suspended Particulates and Fine Particulate Matter from Xi'an, China, J. Air Waste Manage., 58(12), 1560–1570, doi:10.3155/1047-3289.58.12.1560, 2008.

Shen, Z., Cao, J., Arimoto, R., Han, Z., Zhang, R., Han, Y., Liu, S., Okuda, T., Nakao, S. and Tanaka, S.: Ionic composition of TSP and PM2.5 during dust storms and air pollution episodes at Xi'an, China, Atmos. Environ., 43(18), 2911–2918, doi:10.1016/j.atmosenv.2009.03.005, 2009.

Shrivastava, M. K., Lane, T. E., Donahue, N. M., Pandis, S. N. and Robinson, A. L.: Effects of gas particle partitioning and aging of primary emissions on urban and regional organic aerosol concentrations, J. Geophys. Res., 113(D18), D18301–16, doi:10.1029/2007JD009735, 2008.

Shrivastava, M. K., Lipsky, E. M., Stanier, C. O. and Robinson, A. L.: Modeling Semivolatile Organic Aerosol Mass Emissions from Combustion Systems, Environ. Sci. Technol., 40(8), 2671–2677, doi:10.1021/es0522231, 2006.

Stein, U. and Alpert, P.: Factor Separation in Numerical Simulations, J. Atmos. Sci., 50(14), 2107–2115, doi:10.1175/1520-0469(1993)050<2107:fsins>2.0.co;2, 1993.

Strader, R.: Evaluation of secondary organic aerosol formation in winter, Atmos. Environ., 33(29), 4849–4863, doi:10.1016/s1352-2310(99)00310-6, 1999.

Sun, Y. L., Wang, Z. F., Fu, P. Q., Yang, T., Jiang, Q., Dong, H. B., Li, J. and Jia, J. J.: Aerosol composition, sources and processes during wintertime in Beijing, China, Atmos. Chem. Phys., 13(9), 4577–4592, doi:10.5194/acp-13-4577-2013, 2013.

Sun, Y., Wang, Z., Dong, H., Yang, T., Li, J., Pan, X., Chen, P. and Jayne, J. T.: Characterization of summer organic and inorganic aerosols in Beijing, China with an Aerosol Chemical Speciation Monitor, Atmos. Environ., 51(C), 250–259, doi:10.1016/j.atmosenv.2012.01.013, 2012.

Tie, X., Madronich, S., Walters, S. and Zhang, R.: Effect of clouds on photolysis and oxidants in the troposphere, J. Geophys. Res., 108(D20), doi:10.1029/2003jd003659, 2003.

Tie, X., Zhang, Q., He, H., Cao, J., Han, S., Gao, Y., Li, X. and Jia, X. C.: A budget analysis of the formation of haze in Beijing, Atmos. Environ., 100(C), 25–36, doi:10.1016/j.atmosenv.2014.10.038, 2015.

Tsimpidi, A. P., Karydis, V. A. and Zavala, M.: Evaluation of the volatility basis-set approach for the simulation of organic aerosol formation in the Mexico City metropolitan area, Atmos. Chem. Phys., 10(2), 525–546, doi:10.5194/acp-10-525-2010, 2010.

Volkamer, R., San Martini, F., Molina, L. T., Salcedo, D., Jimenez, J. L. and Molina, M. J.: A missing sink for gas-phase glyoxal in Mexico City: Formation of secondary organic aerosol, Geophys. Res. Lett., 34(19), L19807–5, doi:10.1029/2007GL030752, 2007.

Wesely, M. L.: Parameterization of surface resistances to gaseous dry deposition in regional-scale numerical models, Atmos. Environ. (1967), 23(6), 1293–1304, doi:10.1016/0004-6981(89)90153-4, 1989.

Yang, F., Tan, J., Zhao, Q., Du, Z., He, K., Ma, Y., Duan, F., Chen, G. and Zhao, Q.: Characteristics of $PM_{2.5}$ speciation in representative megacities and across China, Atmos. Chem. Phys., 11(11), 5207–5219, doi:10.5194/acp-11-5207-2011, 2011.

Yu, X. Y.: Measurements of Carbonaceous Aerosols Using Semi-Continuous Thermal-Optical Method, InTech. 2011.

Yu, X. Y., Cary, R. A. and Laulainen, N. S.: Primary and secondary organic carbon downwind of Mexico City, Atmos. Chem. Phys., 9(18), 6793–6814, doi:10.5194/acp-9-6793-2009, 2009.

Zhang, Q., Jimenez, J. L., Canagaratna, M. R., Allan, J. D., Coe, H., Ulbrich, I., Alfarra, M. R., Takami, A., Middlebrook, A. M., Sun, Y. L., Dzepina, K., Dunlea, E., Docherty, K., DeCarlo, P. F., Salcedo, D., Onasch, T., Jayne, J. T., Miyoshi, T., Shimono, A., Hatakeyama, S., Takegawa, N., Kondo, Y., Schneider, J., Drewnick, F., Borrmann, S., Weimer, S., Demerjian, K., Williams, P., Bower, K., Bahreini, R., Cottrell, L., Griffin, R. J., Rautiainen, J., Sun, J. Y., Zhang, Y. M. and Worsnop, D. R.: Ubiquity and dominance of oxygenated species in organic aerosols in anthropogenically-influenced Northern Hemisphere midlatitudes, Geophys. Res. Lett., 34(13), L13801, doi:10.1029/2007GL029979, 2007.

Zhang, Q., Quan, J., Tie, X., Li, X., Liu, Q., Gao, Y. and Zhao, D.: Effects of meteorology and secondary particle formation on visibility during heavy haze events in Beijing, China, Sci. Total Environ., 502, 578–584, doi:10.1016/j.scitotenv.2014.09.079, 2015.

Zhang, Q., Streets, D. G. and Carmichael, G. R.: Asian emissions in 2006 for the NASA INTEX-B mission, Atmos. Chem. Phys., 9(14), 5131–5153, doi:10.5194/acp-9-5131-2009, 2009.

Zhang, R., Jing, J., Tao, J., Hsu, S. C., Wang, G., Cao, J., Lee, C. S. L., Zhu, L., Chen, Z., Zhao, Y. and Shen, Z.: Chemical characterization and source apportionment of $PM_{2.5}$ in Beijing: seasonal perspective, Atmos. Chem. Phys., 13(14), 7053–7074, doi:10.5194/acp-13-7053-2013, 2013.

Zhao, J., Levitt, N. P., Zhang, R. and Chen, J.: Heterogeneous Reactions of Methylglyoxal in Acidic Media: Implications for Secondary Organic Aerosol Formation, Environ. Sci. Technol., 40(24), 7682–7687, doi:10.1021/es060610k, 2006.

Table 1 Previous results about different OA contributions

Reference	Time Period	City	Description
Huang et al. (2014)	5–25 January 2013	Beijing Shanghai Guangzhou Xi'an	OA/PM$_{2.5}$ (40.7%) OA/PM$_{2.5}$ (48.0%) OA/PM$_{2.5}$ (33.1%) OA/PM$_{2.5}$ (30.5%)
Sun et al. (2012)	26 June to 28 August 2011	Beijing	OOA/OA (64%)
Sun et al. (2013)	Summer 2012	Beijing	(OA in NR-PM$_1$) / NR-PM$_1$ (52%)
Cao et al. (2013)	MIRAGE-Shanghai 2009	Shanghai	OC/TC (31%)

Table 2 Primary organic carbon and volatile organic compounds emissions from anthropogenic sources in Xi'an and surrounding areas (the area surrounded by the white line in Figure 1c) in April

Anthropogenic Emission Sectors	Primary Organic Carbon (Mg)	Volatile Organic Compounds (Mg)
Industry	2486.0	7634.5
Power Plant	0.0	81.7
Residential	4988.8	1704.4
Transportation	318.5	736.9

Table 3 The primary OC/EC ratios over China in 2003 proposed by Cao et al. (2007)

	Northern Cities		Southern Cities	
	Winter	Summer	Winter	Summer
POC/EC ratio	2.81	1.99	2.10	1.29

Table 4 Simulated mass fractions of SOA in the total OA and the SOA contribution from various formation pathways averaged over the simulation period at urban, rural and background sites

Duration	Site Type	SOA Mass Fraction in OA (%)	Mass Fraction in SOA (%)			
			PSOA[a]	ASOA[b]	BSOA[c]	GSOA[d]
April 23	Urban	32.5	77.9	5.8	5.6	10.6
	Rural	36.3	80.3	5.2	5.1	9.4
	Background	58.6	86.9	4.0	5.4	3.7
April 24	Urban	34.8	80.5	6.0	8.5	5.0
	Rural	39.9	84.4	4.0	8.5	3.1
	Background	74.4	89.4	3.2	5.8	1.6
April 25	Urban	37.3	79.5	6.2	9.9	4.4
	Rural	44.1	80.7	5.3	10.3	3.7
	Background	75.7	89.2	2.4	6.8	1.6

[a] SOA from oxidation and partitioning of POA treated as semi-volatile;
[b] SOA from oxidation of anthropogenic VOCs;
[c] SOA from oxidation of biogenic VOCs;
[d] SOA from irreversible uptake of glyoxal and methylglyoxal on aerosol surfaces.

Table 5 OA concentrations and contributions and OA contributions to $PM_{2.5}$ from anthropogenic emissions averaged over the simulation period at urban, rural, and background sites

	OA Concentration ($\mu g\ m^{-3}$)	OA Contribution (%)	OA contribution to $PM_{2.5}$ (%)
Urban			
Ant.[a]	18.2	82.4	19.2
Res.[b]	10.4	47.2	11.0
Tra.[c]	5.5	25.0	5.8
Ind.[d]	1.3	6.1	1.4
Rural			
Ant.[a]	12.8	77.3	15.8
Res.[b]	7.9	47.8	9.8
Tra.[c]	3.4	20.3	4.1
Ind.[d]	0.4	2.6	0.5
Background			
Ant.[a]	4.7	58.6	19.0
Res.[b]	2.4	30.2	9.8
Tra.[c]	1.6	19.8	6.4
Ind.[d]	0.0	0.0	0.0

[a] Ant. stands for all anthropogenic emissions;
[b] Res. stands for residential emissions;
[c] Tra. stands for transportation emissions;
[d] Ind. stands for industrial emissions.

Figure Captions

Figure 1 Map showing (a) the location of Xi'an in China, (b) WRF-CHEM model simulation domain with topography and (c) geographic distributions of 13 ambient air quality monitoring stations (black triangles) and 29 enhanced sites with filter measurements (squares). The filled red, blue, and green squares represent the urban, rural, and background sites, respectively. The area surrounded by the white line in (c) is defined as Xi'an and surrounding areas. The black circle in (b) and (c) shows the ring expressway of Xi'an. The yellow spot is the location of the Jinghe Meteorological Station.

Figure 2 Geographic distributions of anthropogenic emissions of (a) primary organic aerosol and (b) volatile organic compounds in the simulation domain. The black lines present provincial boundaries in China.

Figure 3 Plot showing the means and standard deviations of observed springtime $PM_{2.5}$ and organic carbon concentrations from 2009 to 2013 (blue), along with the filter measurements during the simulation period in this study (SimPrd, red)

Figure 4 Temporal variations of simulated (blue line) and observed (black dots) meteorological fields including near-surface (a) temperature, (b) relative humidity, (c) wind speed, and (d) wind direction at the Jinghe Meteorological Station which is close to Xi'an from 23 to 25 April 2013.

Figure 5 Spatial patterns of calculated (contours) and observed (squares) O_3 concentrations at 08:00 BJT and 15:00 BJT from 23 to 25 April 2013 along with wind fields (back arrows).

Figure 6 Spatial patterns of calculated (contours) and observed (squares) $PM_{2.5}$ concentrations at 08:00 BJT and 15:00 BJT from 23 to 25 April 2013 along with wind fields (back arrows).

Figure 7 Temporal variations of simulated (blue line) and observed (black dots) (a) O_3 and (b) $PM_{2.5}$ concentrations averaged over 13 monitoring sites in Xi'an and surrounding areas from 23 to 25 April 2013.

Figure 8 Comparisons between the predicted and measured daily (a) $PM_{2.5}$ and (b) elemental carbon mass concentrations at 29 sites from 23 to 25 April 2013. The 1:1, 1:2 and 2:1 lines are plotted as dotted lines.

Figure 9 Spatial distributions of calculated (contours) and observed (squares) daily $PM_{2.5}$ (left column) and EC (right column) concentrations from 23 to 25 April 2013.

Figure 10 Scatter plots of the simulated (a) OA, (b) POA, and (c) SOA from the traditional (blue spots) and non-traditional (red spots) SOA modules against the observations at 29 sites from 23 to 25 April 2013.

Figure 11 Temporal variations of the simulated SOA concentrations from the traditional (blue spots) and non-traditional (red spots) SOA modules in Xi'an and surrounding areas from 23 to 25 April 2013.

Figure 12 Spatial distributions of the NT-SOA module calculated (contours) and filter observed (squares) daily OA (left column), POA (middle column), and SOA (right column) mass concentrations from 23 to 25 April 2013. Red squares in (g), (h), and (i) show the location of the background site.

Figure 13 Comparisons between the NT-SOA module predicted and filter measured daily SOA mass fraction in OA at urban, rural and background sites during the simulation episode.

Figure 14 NT-SOA module simulated contributions of different formation pathways to SOA levels averaged over the simulation episode at (a) urban, (b) rural, and (c) background sites.

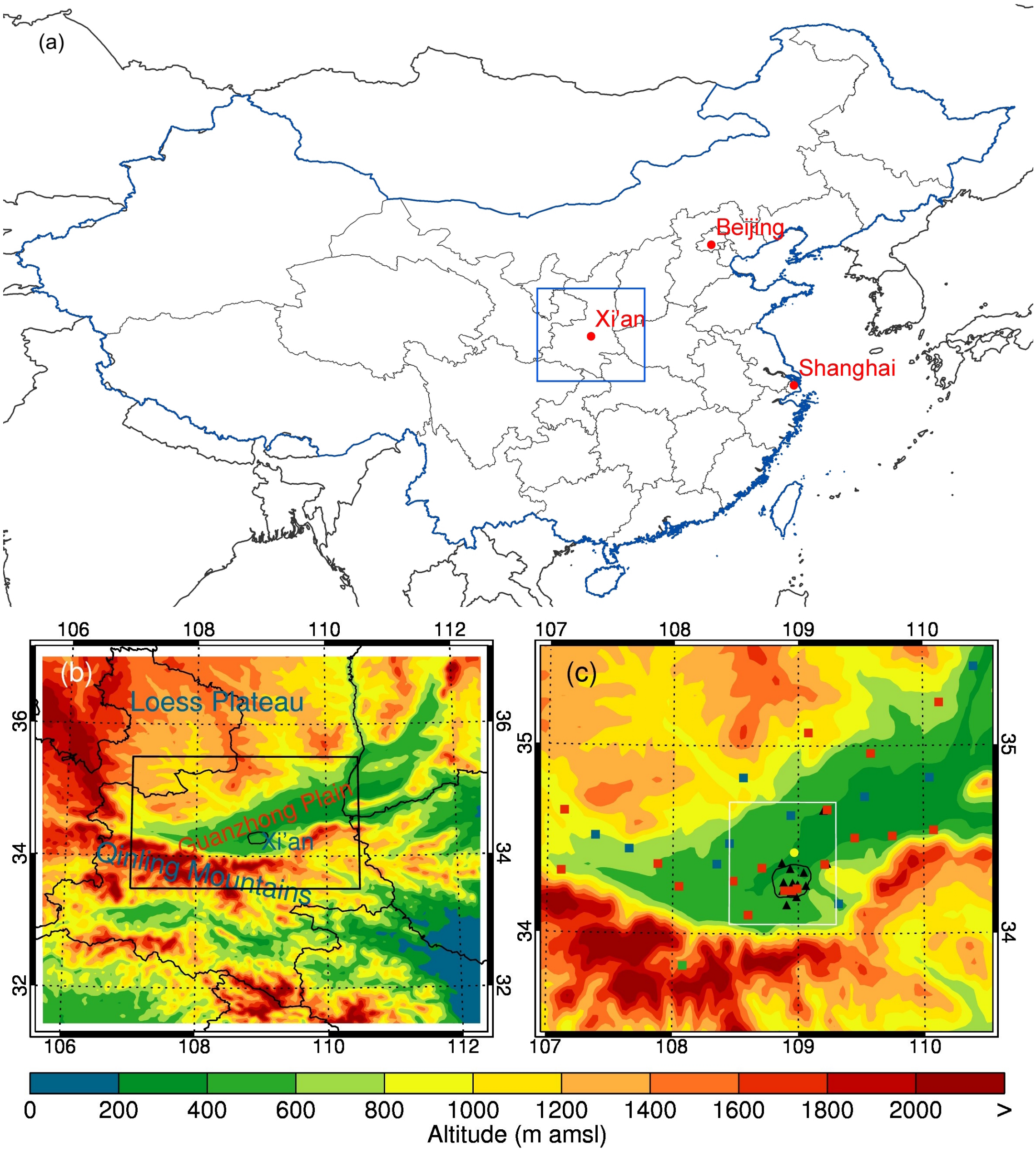
(a)
Beijing
Xi'an
Shanghai
(b)
Loess Plateau
Guanzhong Plain
Xi'an
Qinling Mountains
106
108
110
112
32
34
36
(c)
107
108
109
110
34
35
0
200
400
600
800
1000
1200
1400
1600
1800
2000
>
Altitude (m amsl)

Figure 1

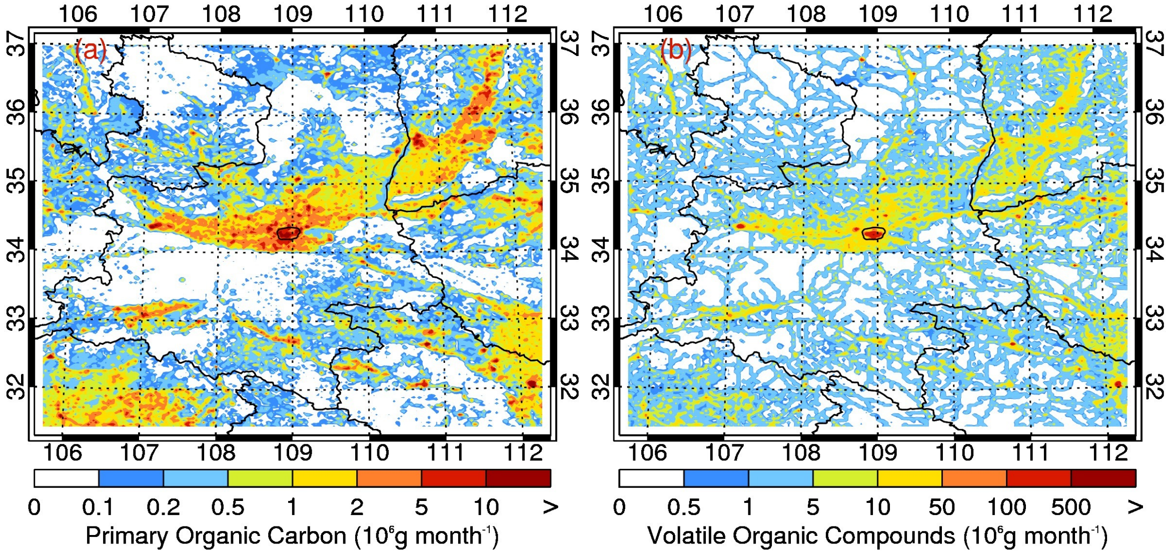
(a)
(b)
106
107
108
109
110
111
112
32
33
34
35
36
37
0
0.1
0.2
0.5
1
2
5
10
>
Primary Organic Carbon (10^6g month^{-1})
0
0.5
1
5
10
50
100
500
>
Volatile Organic Compounds (10^6g month^{-1})

Figure 2

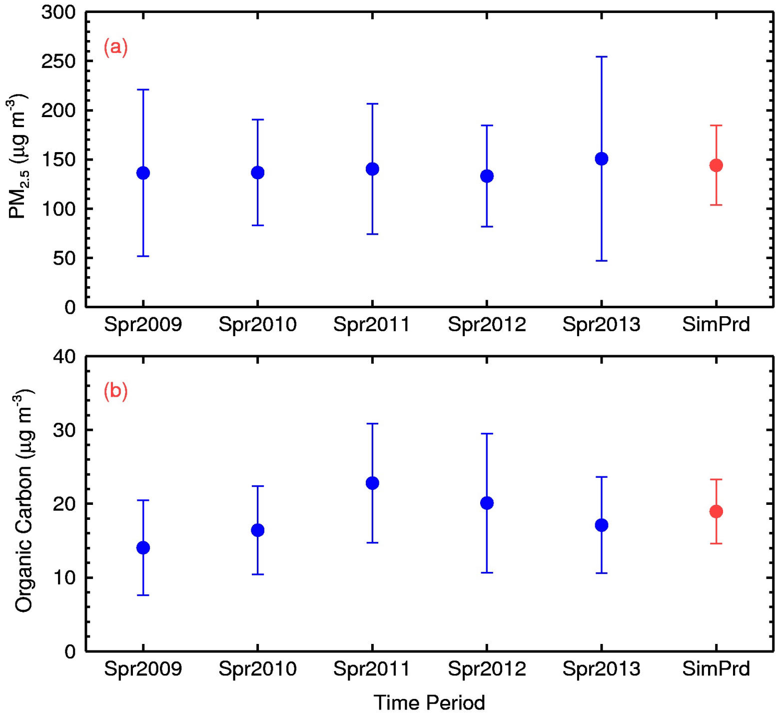

807

808 Figure 3

809

810

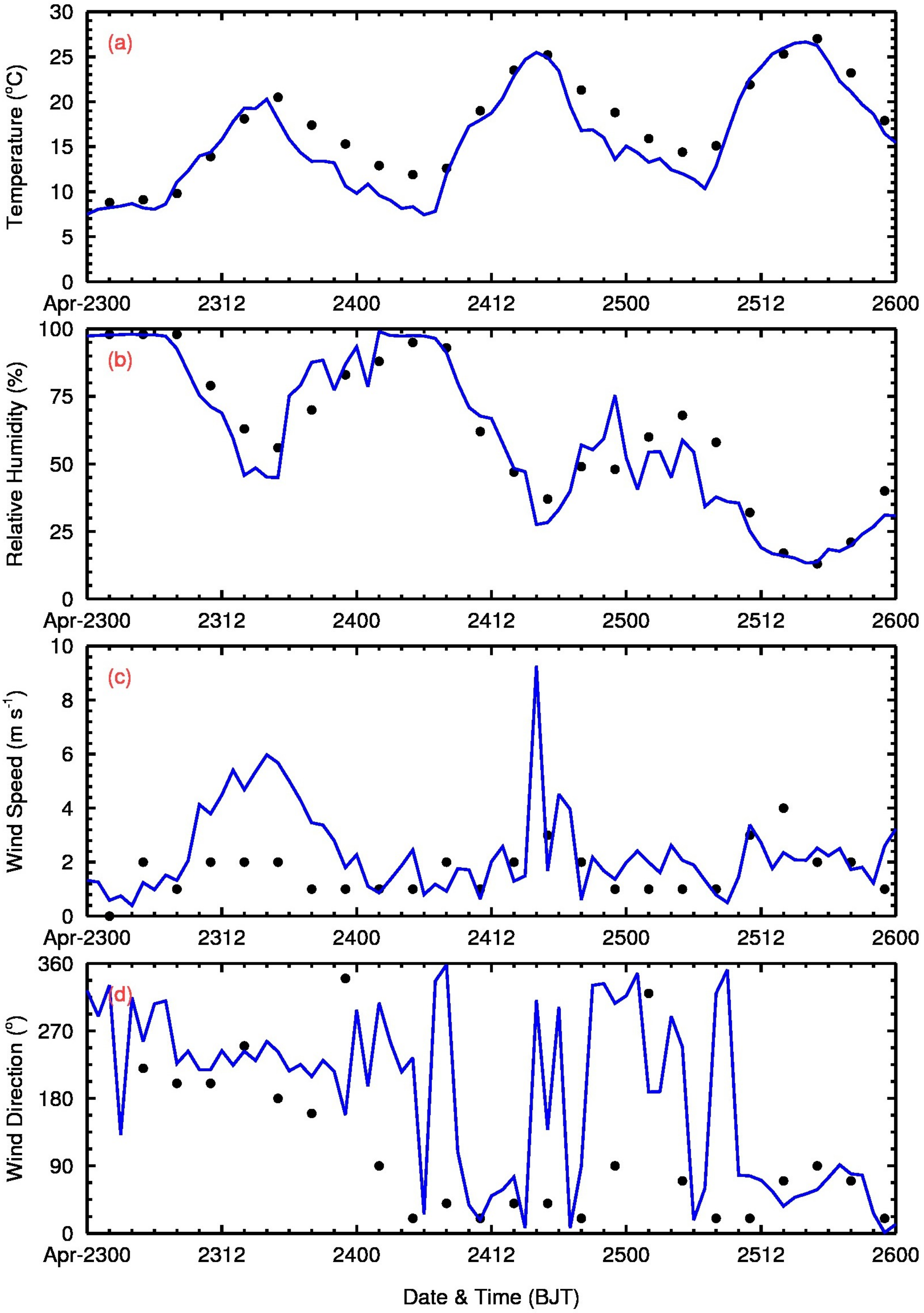
(a)
Temperature (°C)
30
25
20
15
10
5
0
Apr-2300
2312
2400
2412
2500
2512
2600
(b)
Relative Humidity (%)
100
75
50
25
0
(c)
Wind Speed (m s-1)
10
8
6
4
2
0
(d)
Wind Direction (°)
360
270
180
90
0
Date & Time (BJT)

Figure 4

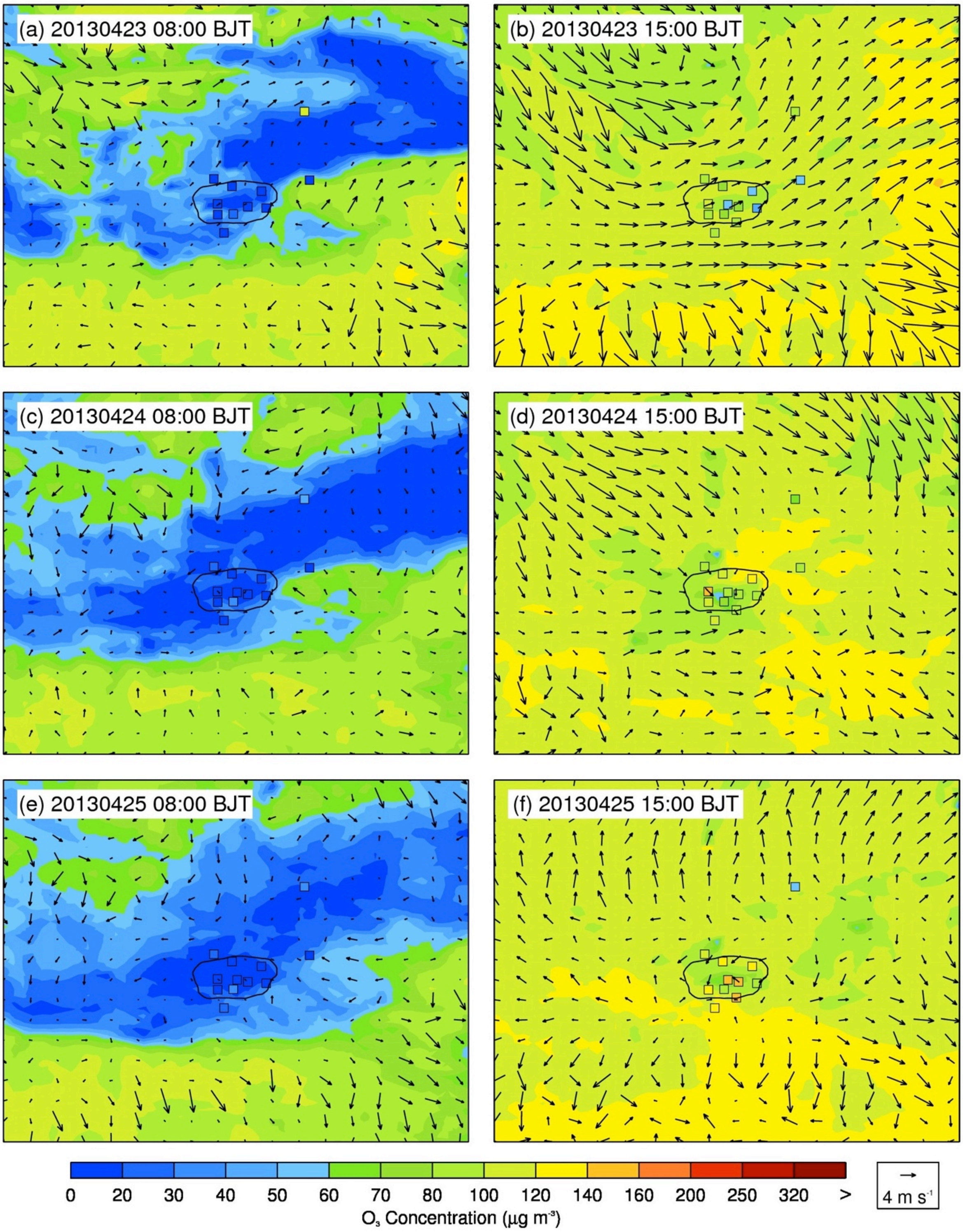
(a) 20130423 08:00 BJT
(b) 20130423 15:00 BJT
(c) 20130424 08:00 BJT
(d) 20130424 15:00 BJT
(e) 20130425 08:00 BJT
(f) 20130425 15:00 BJT
0
20
30
40
50
60
70
80
100
120
140
160
200
250
320
>
O₃ Concentration (μg m⁻³)
4 m s⁻¹

Figure 5

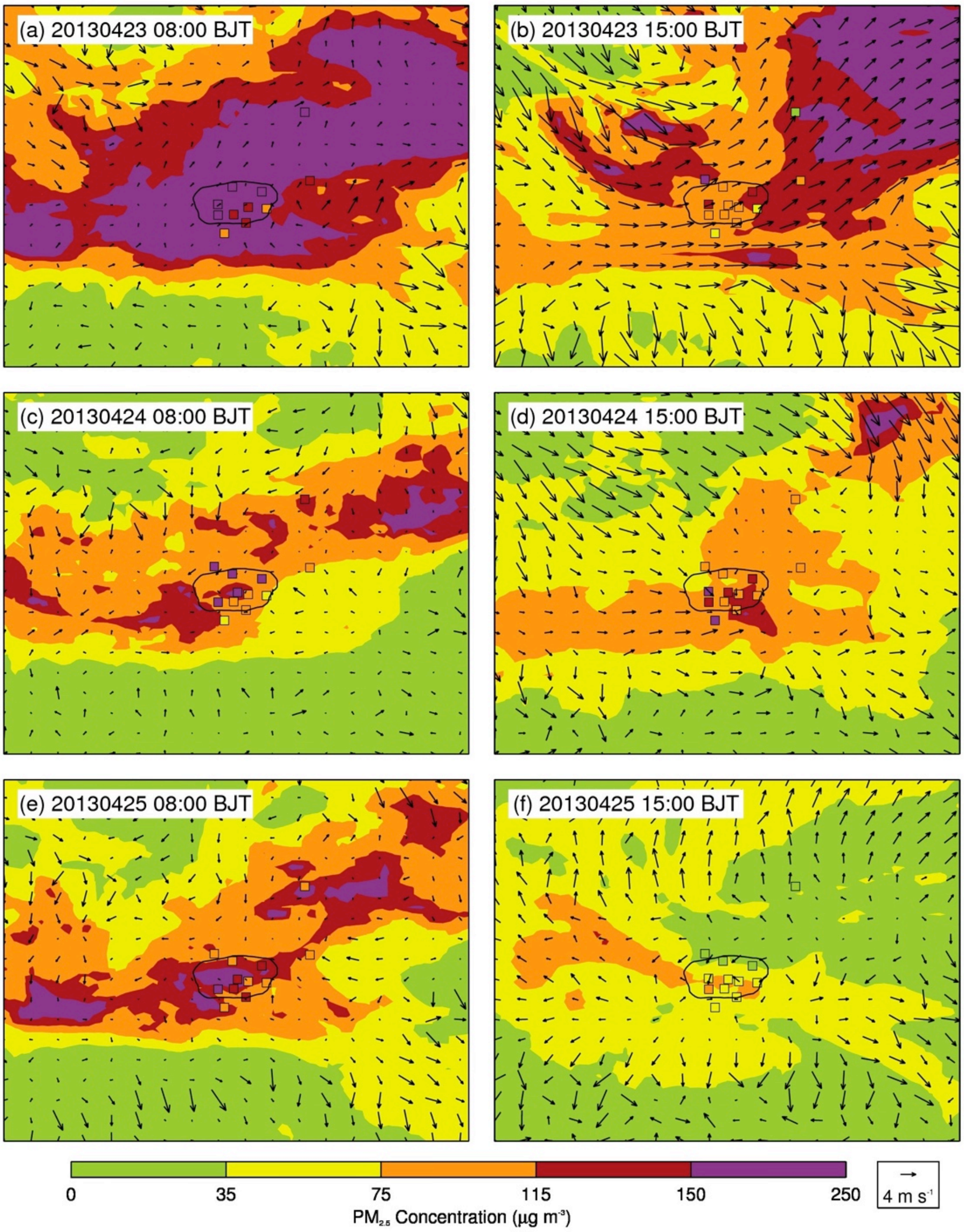
(a) 20130423 08:00 BJT
(b) 20130423 15:00 BJT
(c) 20130424 08:00 BJT
(d) 20130424 15:00 BJT
(e) 20130425 08:00 BJT
(f) 20130425 15:00 BJT
0
35
75
115
150
250
PM2.5 Concentration (μg m-3)
4 m s-1

Figure 6

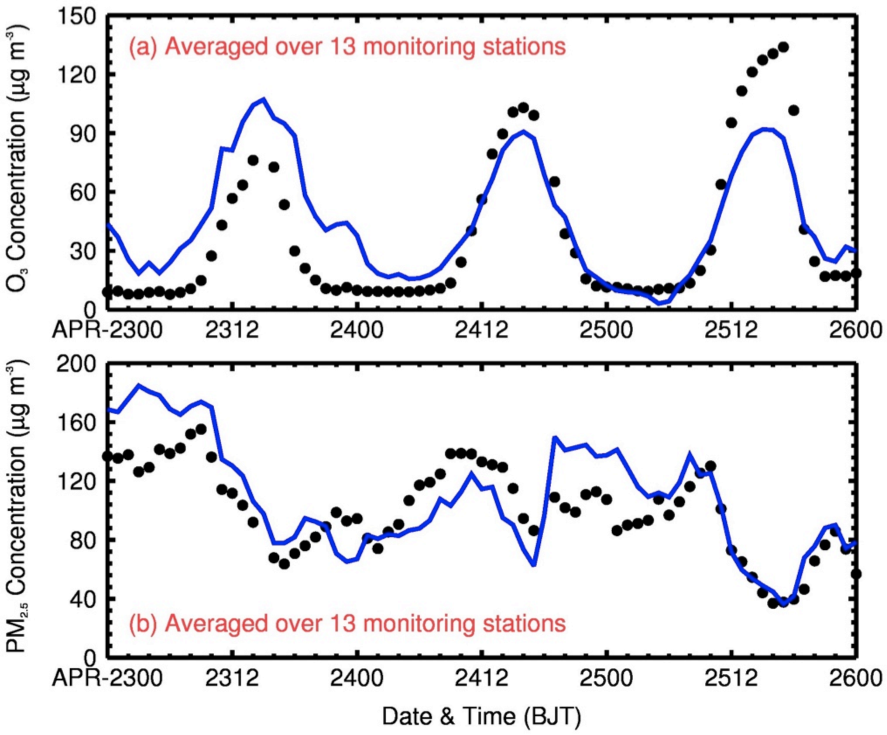

(a) Averaged over 13 monitoring stations
O$_3$ Concentration (μg m^{-3})
0
30
60
90
120
150
APR-2300
2312
2400
2412
2500
2512
2600
(b) Averaged over 13 monitoring stations
PM$_{2.5}$ Concentration (μg m^{-3})
0
40
80
120
160
200
APR-2300
2312
2400
2412
2500
2512
2600
Date & Time (BJT)

Figure 7

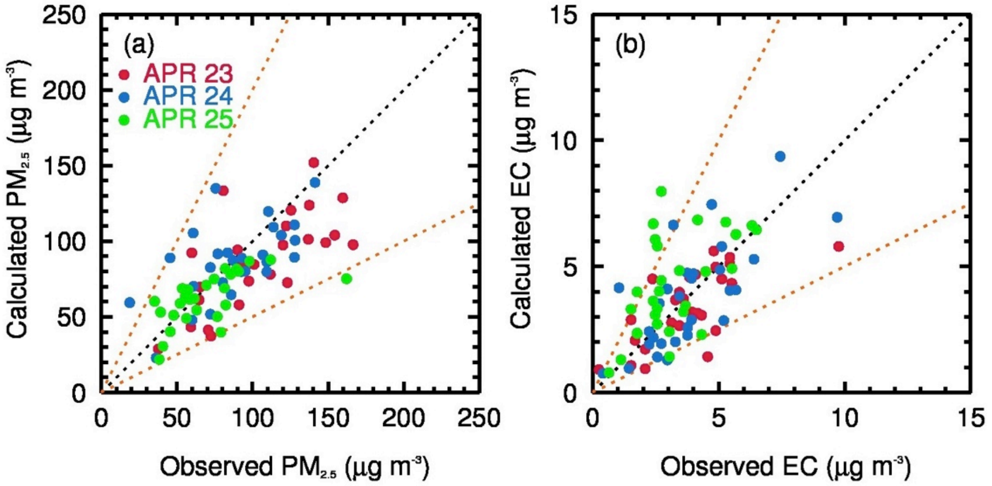
(a)
APR 23
APR 24
APR 25
Calculated PM2.5 (μg m-3)
Observed PM2.5 (μg m-3)
0
50
100
150
200
250
(b)
Calculated EC (μg m-3)
Observed EC (μg m-3)
0
5
10
15

Figure 8

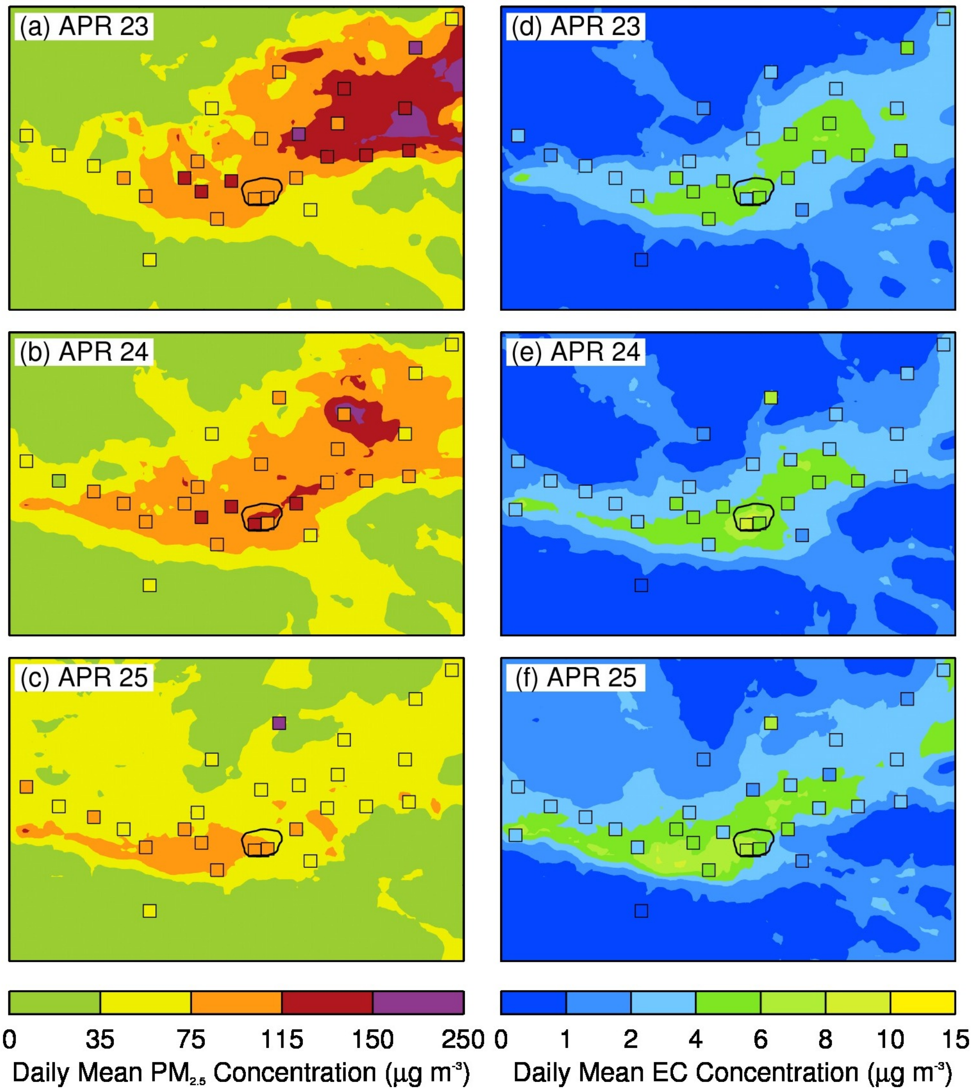
(a) APR 23
(b) APR 24
(c) APR 25
(d) APR 23
(e) APR 24
(f) APR 25
0
35
75
115
150
250
Daily Mean PM$_{2.5}$ Concentration (μg m^{-3})
0
1
2
4
6
8
10
15
Daily Mean EC Concentration (μg m^{-3})

Figure 9

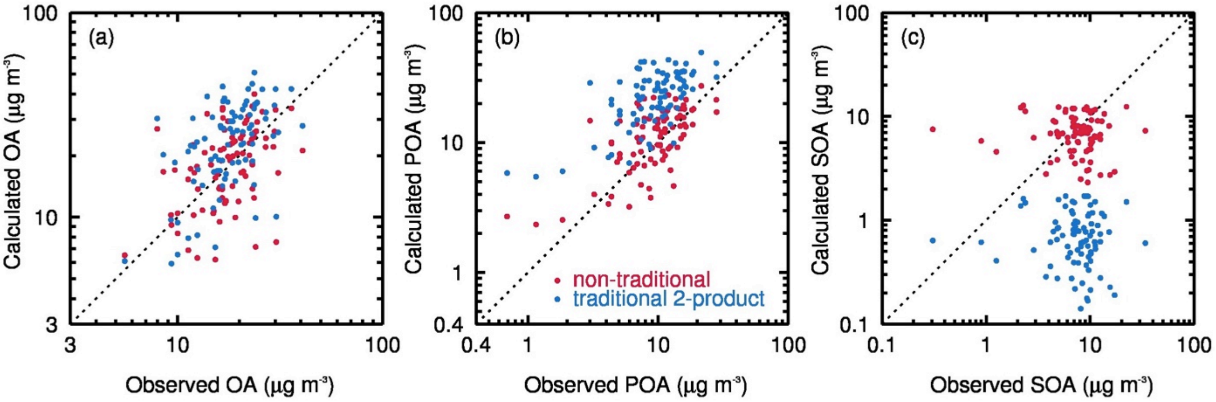
(a)
Calculated OA (µg m⁻³)
Observed OA (µg m⁻³)
100
10
3
3
10
100
(b)
Calculated POA (µg m⁻³)
Observed POA (µg m⁻³)
100
10
1
0.4
0.4
1
10
100
non-traditional
traditional 2-product
(c)
Calculated SOA (µg m⁻³)
Observed SOA (µg m⁻³)
100
10
1
0.1
0.1
1
10
100

Figure 10

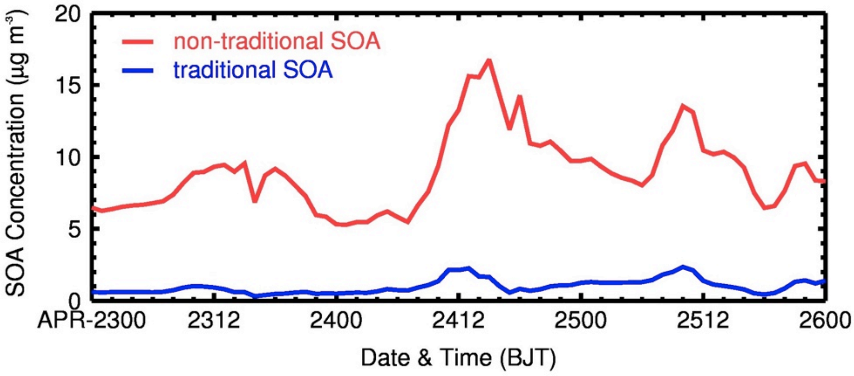
non-traditional SOA
traditional SOA
SOA Concentration (μg m^{-3})
0
5
10
15
20
APR-2300
2312
2400
2412
2500
2512
2600
Date & Time (BJT)

Figure 11

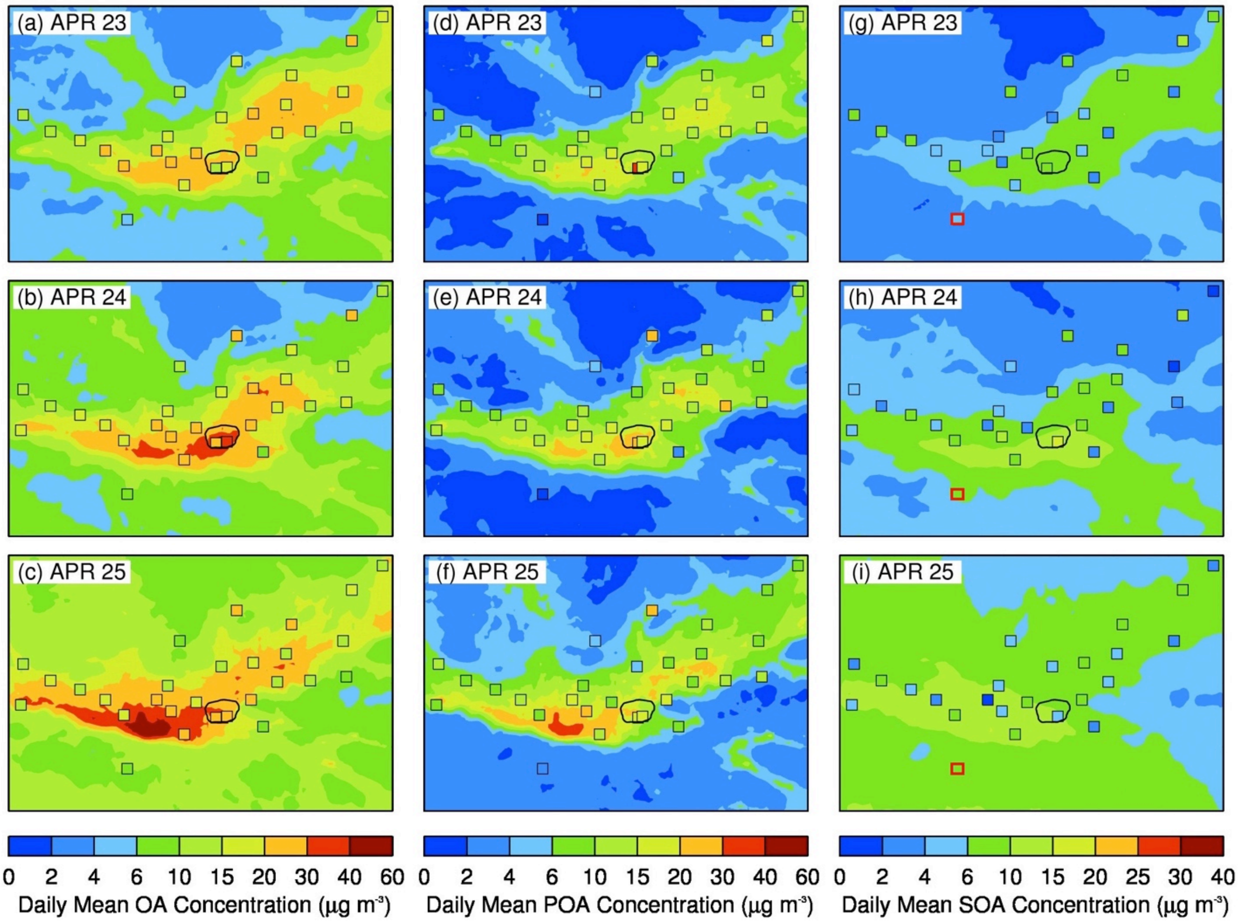
(a) APR 23
(d) APR 23
(g) APR 23
(b) APR 24
(e) APR 24
(h) APR 24
(c) APR 25
(f) APR 25
(i) APR 25
0 2 4 6 10 15 20 30 40 60
Daily Mean OA Concentration (µg m⁻³)
0 2 4 6 10 15 20 30 40 60
Daily Mean POA Concentration (µg m⁻³)
0 2 4 6 10 15 20 25 30 40
Daily Mean SOA Concentration (µg m⁻³)

Figure 12

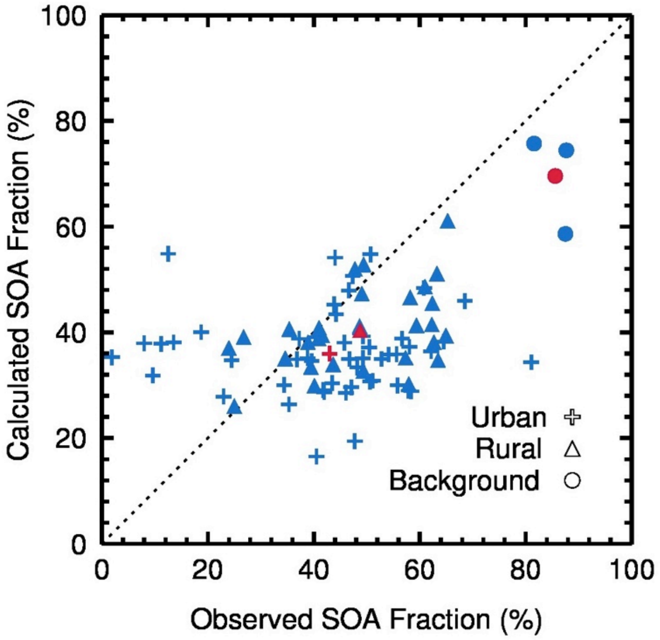
Calculated SOA Fraction (%)
Observed SOA Fraction (%)
0
20
40
60
80
100
Urban ✚
Rural △
Background ○

Figure 13

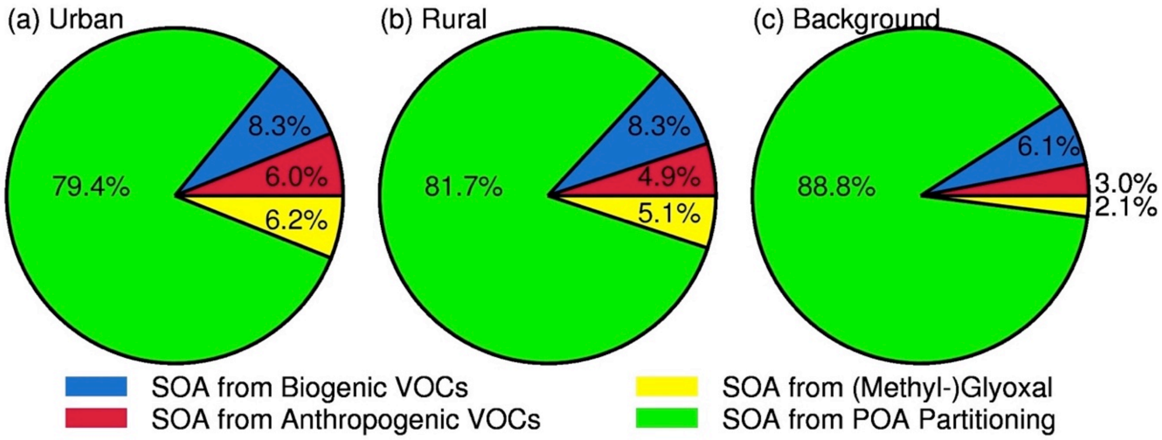
(a) Urban
8.3%
6.0%
6.2%
79.4%
(b) Rural
8.3%
4.9%
5.1%
81.7%
(c) Background
6.1%
3.0%
2.1%
88.8%
SOA from Biogenic VOCs
SOA from Anthropogenic VOCs
SOA from (Methyl-)Glyoxal
SOA from POA Partitioning

Figure 14